

Structure and magnetic properties of monovalent doping charge ordering perovskite

H. Trabelsi

Laboratory of Applied Physics, Faculty of Sciences of Sfax, B.P. 1171, 3000 Sfax, University of Sfax, Tunisia

Corresponding author: email: hamdi.trabelsi@outlook.fr

Received date: Feb. 03, 2018; revised date: Feb. 16, 2018; accepted date: Feb. 22, 2018

Abstract

The present paper reports detailed structural, magnetic and magnetocaloric characterizations of the charge ordered $Nd_{0.5}Ca_{0.5}M_{0.1}MnO_3$ ($M=Na, K$: NCNMO and NCKMO) polycrystalline samples. Our compounds were synthesized using the solid state reaction at high temperature. Both samples are single phase and crystallize in the orthorhombic structure with $Pnma$ space group. NCNMO ($\langle r_A \rangle = 1.1775 \text{ \AA}$) undergoes a charge disordering transition (CO) associated to the paramagnetic (PM)-antiferromagnetic (AFM) phase transition at $T < 250 \text{ K}$. The long range AFM ordering seems to form at 35 K , rather than 150 K as previously reported. In the intermediate temperature range, charge ordering occurs while orbital ordering sets in progressively, with no magnetic order. For NCKMO sample ($\langle r_A \rangle = 1.2085 \text{ \AA}$), K doping induces the melting of the CO state and the presence of the short-range AFM phase, which is metastable and transforms into the stable ferromagnetic (FM) state. Magnetic characterization shows the signature of AFM-FM ordering and spin-glass coexisting at low temperature. The temperature dependence of magnetic entropy change at high magnetic field values presents some anomalies attributed to the metamagnetic transition, which is of first order.

Keywords: Neodymium calcium manganite; Monovalent doping; Structure; Charge ordering; Magnetocaloric effect.

1. Introduction

Over the last fifteen years, hole-doped manganites $R_{1-x}A_xMnO_3$ have attracted considerable research attention due to their rich variety of physical phenomena and potential application [1-3]. The double-exchange (DE) interaction between Mn^{3+} and Mn^{4+} ions via the intervening ligand O ion leads to a FM metallic or insulating phase in the manganites, whereas super exchange interaction between Mn^{3+} - Mn^{3+} and Mn^{4+} - Mn^{4+} results into AFM ordering. For different choices of A-site trivalent and divalent materials and x values, the average A-site ionic radius of the compound, $\langle r_A \rangle$, changes significantly, modifying the MnO_6 octahedra and thus altering the FM and AFM interaction. For a better understanding of the mechanisms behind these oxides, considerable work has recently been done on the CO systems [4-6]. The spatial CO phase, which can quite easily be observed in half-doped manganites $R_{0.5}A_{0.5}MnO_3$ ($R = La, Pr, Nd$; $A = Sr, Ca$), behaves as the periodic arrangement of Mn^{3+}/Mn^{4+} ions.

Generally, the CO formation is accompanied by an AFM phase transition. By way of example, $La_{0.5}Ca_{0.5}MnO_3$ is a ferromagnetic in the temperature regime $T_{CO} < T < T_C$ ($T_{CO} = 190 \text{ K}$, $T_C = 230 \text{ K}$) but transforms into a CO AFM insulator at temperatures below T_{CO} [7]. Similarly, $Pr(Nd)_{0.5}Sr_{0.5}MnO_3$ exists as a FM metallic state below 250 K and becomes a CO AFM insulator at 150 K [8, 9]. It is well confirmed that the CO state originates from the

interplay between Coulomb repulsion, orbital ordering and Jahn-Teller distortion. $Nd_{0.5}Ca_{0.5}MnO_3$ ($\langle r_A \rangle = 1.1715 \text{ \AA}$) is a typical CO system which transforms into the CO state at 250 K and undergoes a PM to AFM phase transition at 150 K [10, 12]. Interestingly, after entering into CO AFM state, its magnetization tends to increase rather than decrease, especially below 100 K . This behavior has initially been attributed to the PM contribution of Nd^{3+} ions; however, this conjecture turned out to be inconsistent with theory [13]. Gordon et al. suggested instead that a coupling between the Nd and Mn spins is responsible for the observed anomaly [14]. While the intrinsic mechanism for this behavior is still very unclear, further investigations provided interesting new insight.

In $Nd_{0.5}Ca_{0.5}MnO_3$ thin films, Guha et al. disclosed a threshold which is associated with the onset of a nonlinear electrical conduction, and suggested that this is caused by a depinning of the CO state [15]. Moreover, the properties of manganites are strongly affected by chemical factors such as average cationic radius $\langle r_A \rangle$ in the A site [16-18] and the A-site cationic size mismatch [19, 20] quantified by $\sigma^2 = \sum_i y_i r_i^2 - \langle r_A \rangle^2$ (y_i is the fractional occupancy of A-site ions, and r_i is the corresponding ionic radius). This implies that A-site substitution gives potentially interesting new insights into $Nd_{0.5}Ca_{0.5}MnO_3$; on the other hand, it must be noted that the ratio of Mn^{4+}/Mn^{3+} is changed by this doping method, and this is directly associated to the long-range CO formation. The aim of our study is to investigate the change in magnetic behavior arises as a

consequence of the slight increase of the average ionic radius ($\langle r_A \rangle$) by adding small amounts of monovalent cation to the charge ordered neodymium calcium manganite, such as Na and K, which their ionic radius are larger than that of Nd and Ca.

2. Experimental details

2.1. Samples preparation

Polycrystalline $\text{Nd}_{0.5}\text{Ca}_{0.4}\text{M}_{0.1}\text{MnO}_3$ ($M=\text{Na}, \text{K}$) samples were prepared by the standard solid-state reaction processing[21]. The well-mixed stoichiometric powder with high-purity (>99.9%) Nd_2O_3 , CaCO_3 , MnO_2 , Na_2CO_3 and K_2CO_3 were calcined at 800 °C for 12 hours. Then the as-obtained powders were pressed into pellets (of about 2 mm thickness and 13 mm diameter) and sintered at 1000 °C in air for 48 hours, then furnace-cooled to room temperature.

2.2. Characterization techniques

Phase purity, homogeneity and cell dimensions were determined by powder X-Ray diffraction at room temperature. Structural analysis was performed using the standard Rietveld technique [22, 23]. The amount of Mn^{4+} ions has been quantitatively checked by chemical analysis. Scanning electron microscopy (SEM) was performed to examine the surface morphology of the samples. Magnetization measurements versus temperature and versus magnetic applied field were carried out using a SQUID magnetometer for both samples.

3. Results

Structural investigations were carried out at room temperature by powder XRD and the data were analyzed using the Rietveld profile-fitting method. The profile refinement is started with scale and background parameters followed by the unit cell parameters. Then the peak asymmetry and preferred orientation corrections are applied. Finally, the positional parameters and the individual isotropic parameters are refined. Fig. 1 shows typical refined diagrams of NCNMO and NCKMO samples. It was found that all samples are single phase without any detectable impurity and crystallize in the orthorhombic system with Pnma space group. Further, using the refined patterns the unit cell volume, bond lengths, bond angles, the average ionic radius in the A site ($\langle r_A \rangle$) and the cationic disorder σ^2 were computed and are presented in Table 1.

The average crystallite size can be estimated from the XRD data using the Scherer relation as follows [24, 25]:

$$D_{\text{XRD}} = K\lambda/\beta\cos\theta$$

Eq.1where K , λ , θ and β are the grain shape factor, the X ray

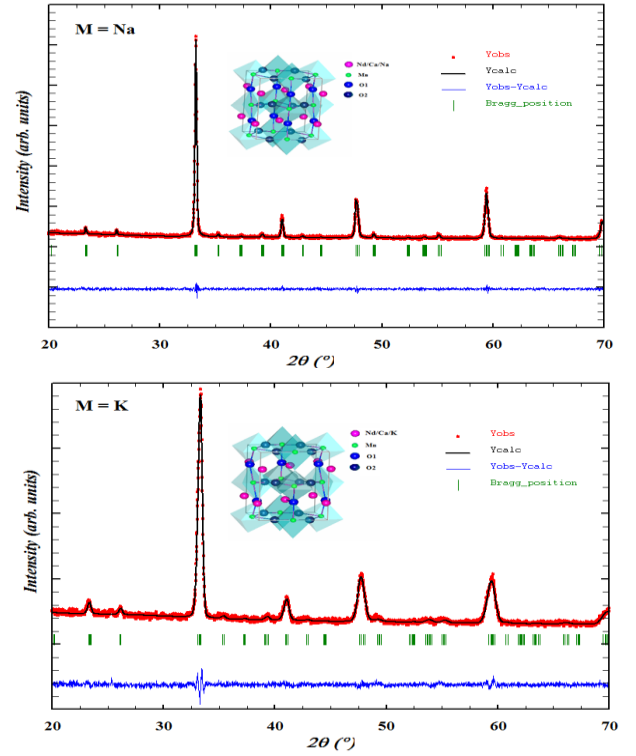


Figure 1. Structures and X-Ray diffraction patterns at room temperature of NCNMO and NCKMO samples.

wavelength, the Bragg diffraction angle, and the full width at half maximum (FWHM) of the diffraction peak, respectively. The values of the effective particle size are summarized in Table 1.

We observe, with increasing average ionic radius in the A site ($\langle r_A \rangle$), a small decrease of the $\langle \text{Mn-O-Mn} \rangle$ angle. This result can be explained by the sodium ionic radius (1.24 Å), which is smaller than that of potassium (1.55 Å). Monovalent ions radius induce local distortions of the $\langle \text{Mn-O-Mn} \rangle$ angle in the system and consequently cause a random distribution of the magnetic exchange interactions. The internal stress caused by monovalent substitution may result in a larger rotation of the MnO_6 octahedra.

Table 1: Crystallographic data of NCNMO and NCKMO manganites.

Sample	NCNMO	NCKMO
V (Å ³)	221.188	221.285
$\langle \text{Mn-O} \rangle$ (Å)	1.949	1.982
$\langle \text{Mn-O-Mn} \rangle$ (°)	155.775	152.655
$\langle r_A \rangle$ (Å)	1.1775	1.2085
σ^2 (Å ²)	$4.982 \cdot 10^{-1}$	$13.022 \cdot 10^{-3}$
D_{XRD} (nm)	65.81	19.74
Goodness of fit χ^2 (%)	1.33	1.45

The value of the tolerance factor [26] is 0.932 and 0.943 for NCNMO and NCKMO samples, respectively. For $t < 1$, the A cation is too small and it will generally be energetically favorable to undergo octahedral tilting distortions to optimize the A-O interactions.

The structures of $\text{Nd}_{0.5}\text{Ca}_{0.4}\text{M}_{0.1}\text{MnO}_3$ ($M=\text{Na}, \text{K}$) (given by FullProf software's Fp Studio Ver-2.0) are shown inset Fig. 1.

As ours samples have been synthesized in air, they are stoichiometric in oxygen [27]. For both compounds the $\text{Mn}^{4+}/\text{Mn}^{3+}$ amount is theoretically equal to $3/2$. The Mn^{4+} and Mn^{3+} contents have been checked by chemical analysis, (Table 2). We can notice a slight discrepancy between experimental and theoretical results. $\text{Mn}^{4+}/\text{Mn}^{3+}$ ratio is equal to 1.49 and 1.54 for the NCNMO and NCKMO samples respectively.

Table 2: Chemical analysis results for NCNMO and NCKMO samples.

Sample	Experimental contents	
	Mn^{3+}	Mn^{4+}
NCNMO	40.15%	59.85%
NCKMO	39.39%	60.61%

The morphology and the particle size of $\text{Nd}_{0.5}\text{Ca}_{0.4}\text{M}_{0.1}\text{MnO}_3$ ($M=\text{Na}, \text{K}$) compounds, revealed by SEM, are shown in Fig. 2. The SEM micrographs show that all the grains are multi-faceted, with an average size of $0.41 \mu\text{m}$ and $0.21 \mu\text{m}$ for NCNMO and NCKMO samples respectively. The grain sizes obtained by SEM (D_{SEM}) are much larger than those calculated by the broadening of the diffraction peaks (D_{XRD}), which indicates that each grain observed by SEM basically consists of several crystallites [28].

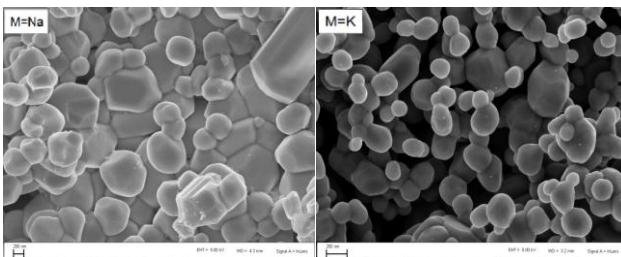


Figure 2. SEM images of NCNMO and NCKMO samples.

Fig. 3 shows the temperature dependence of magnetization and its derivate, measured under an applied magnetic field of 0.05 T in field cooling (FC) conditions for both samples.

For the sodium substituted sample, when the temperature is lowered from room temperature, magnetization first increase due to the formation of a FM phase, but this tendency toward the FM order is destroyed by CO that favors AFM. The $M(T)$ curve measured

under FC condition shows that a notable peak exists near 250 K due to CO phase just as for $\text{Nd}_{0.5}\text{Ca}_{0.3}\text{MnO}_3$ and other systems [29, 30]. Around $T=160\text{K}$ Neel transition (T_N), a discernible kink is also observed, which indicates the onset of the AFM ordering.

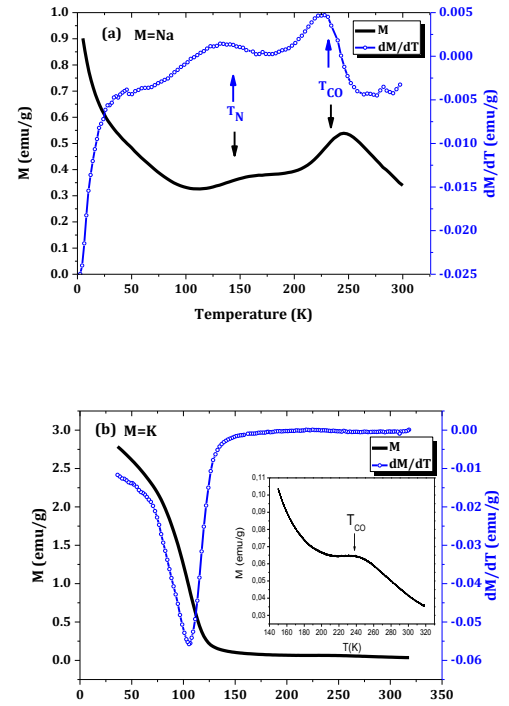


Figure 3. Temperature dependence of magnetization and its derivate for (a) NCNMO and (b) NCKMO manganites at a magnetic applied field of 0.05T. Inset a zoom in the $M(T)$ curve close to the charge ordering transition for the potassium substituted sample.

In the case of K-substituted sample, the temperature dependence of magnetization is distinctly different from Na-substituted counterpart. When the temperature is lowered from room temperature, the magnetization curve shows a weak inflection around 250 K, which is attributed to the onset of transition into the AFM CO state (as shown in the inset). When the temperature is further decreased, the magnetization increases considerably by signaling the onset of a FM phase. It can be seen from the Fig. 3 (b) that NCKMO sample undergoes FM transition at $T_c=105 \text{ K}$. This transition is not sudden but there is a small hump in the magnetization behavior, which indicates that it is an inhomogeneous FM state.

In order to support the magnetization studies and to get more information about the magnetic nature of these charge ordered samples, the temperature variation of field cooled and zero field cooled (ZFC) magnetization studies were also carried out and typical plots for both NCNMO and NCKMO samples are shown in Fig. 4.

For the sodium substituted sample, it can be seen from the figure that when the temperature is lowered from room temperature, both ZFC and FC magnetization increases in the beginning exhibiting a CO transition (T_{co}). Below T_{co} ,

it is notable that the ZFC and FC magnetization curves start to separate from each other at a temperature around 220 K, where a strong irreversibility begins to develop. When the temperature is further decreased below T_N the magnetization increases considerably by signaling the onset of orbital ordered state.

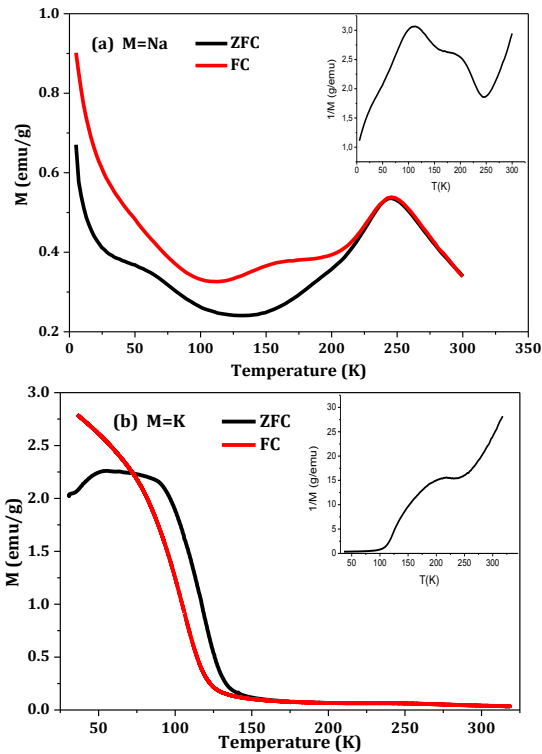


Figure 4. Field cooled and zero field cooled temperature dependent magnetization curves for (a) NCNMO and (b) NCKMO manganites. Insets the temperature dependence of the inverse magnetization ($1/M$) of both samples.

For the NCKMO sample, at low temperature, the FM super-exchange interaction between the residual neighboring Mn^{3+} and Mn^{4+} ions takes place, which results in the rapid increase of magnetization and the strong irreversibility between the ZFC and FC curves. With increasing temperature, the ZFC magnetization starts to increase, reaching a maximum where FM clusters in the AFM matrix grow larger and these FM domains are oriented along the external field. The bifurcation between ZFC and FC magnetization curve is an indication of the glassy behavior [31, 32], which originates from the frustration between the FM order in the clusters with the AFM interactions present in the background matrix. When the temperature is higher than 140 K, it is interesting to notice that no deviation is observed and both the curves are found to coincide with each others. The slight non-zero background signal at high temperatures indicates a weak charge and orbital ordering which has also been observed earlier [33]. Similar to the inverse magnetization curves as observed in the NCNMO sample, the curve for NCKMO sample is also separated into two parts, which implies that the CO phase persists.

With increasing the average cationic radius ($\langle r_A \rangle$) in the A site, the peak around 250 K is gradually broadened and the CO state starts to melt. In fact, whatever ($\langle r_A \rangle$) and the manganese valency are, the increase of σ^2 tends to suppress the magnetic interactions, FM or AFM, and destabilize the CO [34, 35]. These behaviors show the great complexity of the relationships between the chemical factors ($\langle r_A \rangle$ and σ^2) and the magnetic properties of manganites.

The evolution of magnetization versus magnetic applied field at several temperatures for both samples was reported in Fig. 5 in the range 30-300 K. The measurements confirm the existence of different magnetic states as a function of temperature and confirm the results obtained for the M versus T curves.

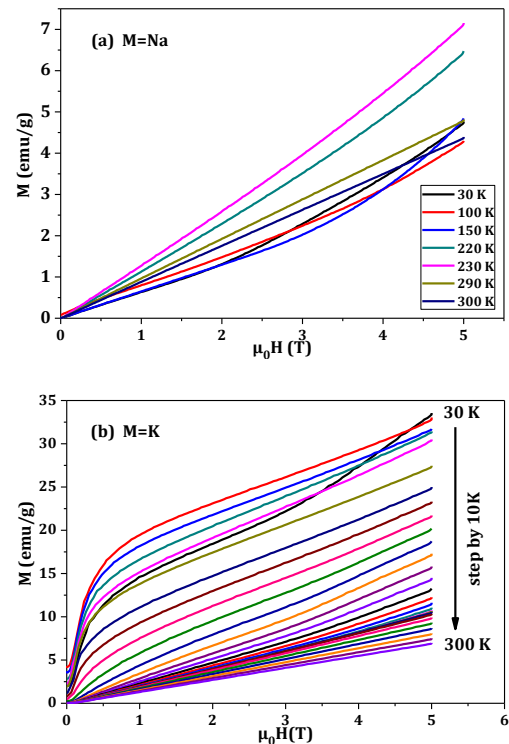


Figure 5. Isothermal magnetization curves at various temperatures for (a) NCNMO and (b) NCKMO manganites.

For NCNMO sample the data were taken at 10 K intervals but we have shown the curves only at selected temperatures just for clarity. While M is linear in H above T_{co} , M (H) at 230 K ($<T_{co}$) shows a tendency to increase rapidly above 1 T. This rapid increase in M, which is incomplete due to the limitation of the available field, is caused by partial suppression of AFM fluctuations in the charge ordered phase. As the temperature decreases below 200 K, M becomes linear with H up to the maximum field since the available field is insufficient to destabilize the CO-type AFM phase.

However, the M (H) of NCKMO compound shows a rapid rise below 1 T followed by a gradual increase with the field up to 5 T. In addition, M (H) are not found to saturate even at 5 T indicating that higher magnetic field

(>5T) might be essential for saturation. Magnetic field dependence of magnetization at 30 K for the potassium substituted sample shows the external field-induced first-order metamagnetic transition from AFM to FM phase. As we can see, $M(H)$ curves for the NCKMO sample are not linear for $T > T_c$. This behavior confirms that the K-substituted sample is not completely PM above T_c and can be attributed to the coexistence of PM and AFM domains. The appearance of a metamagnetic transition for the potassium substituted sample is a clear signature of the coexistence of FM and AFM-CO phases. Indeed, the origine of this steplike transition is the scenario of phase separation, in which the CO AFM and FM phases coexist in the sample and FM phase develops in the CO AFM matrix [36]. There is a considerable competition between these two phases.

To calculate the change in magnetic entropy (ΔS_M) we used the isothermal magnetization measurements at discrete field intervals (Fig. 5). The $\Delta S_M(T, H)$ was calculated by the Maxwell relation [37].

$$\Delta S_M = \int [\partial M / \partial T] dH \quad \text{Eq.2}$$

where M is the magnetization, we have found the derivative $\partial M / \partial T$, and substituted it in the equation (2) [38-40].

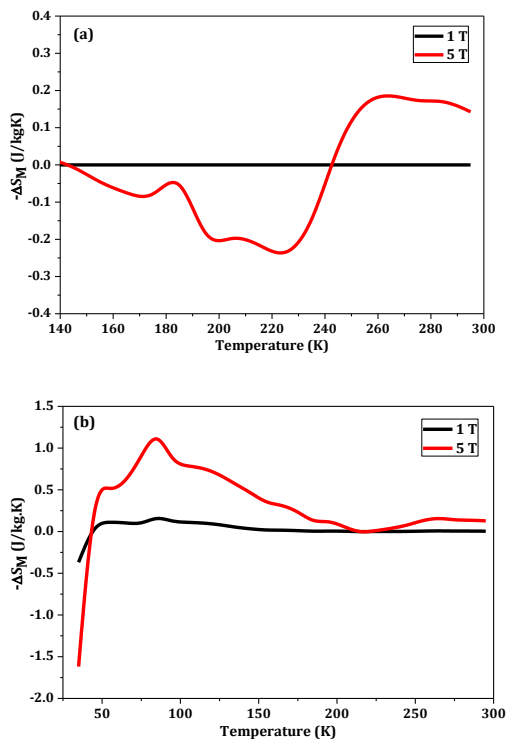


Figure 6. Temperature dependence of magnetic entropy change for: (a) NCNMO, (b) NCKMO samples.

Fig. 6 shows the temperature dependence of the magnetic entropy change ($-\Delta S_M$) taken at magnetic applied fields of 1T and 5T for NCNMO and NCKMO samples. For both compounds, $|\Delta S_M|$ increases with increasing magnetic applied field. NCNMO sample shows a positive entropy change around T_N and T_{CO} due to dominance of

the AFM interactions (i.e. inverse MCE) [38, 39]. With increasing both the temperature and the strength of the applied magnetic field the FM spins start to align, leading to a second negative maximum around 265 K. In addition, we can observe some anomalies in the curve only for the 5T value of magnetic applied field. We can notice the appearance of other maximums of magnetic entropy change. The NCKMO sample exhibits a broad negative peak around T_c (i.e. normal MCE). The normal MCE arises from FM exchange interaction between Mn spins. As well, the change in magnetic entropy curve shows some anomalies. These anomalies can be explained as metamagnetic transition: in fact, PM and AFM coexist above T_c . The application of a strong magnetic field forces the spins to be lined up with field implying the conversion of AFM domains to FM ones. Many compounds, previously studied, exhibit some anomalies in the magnetocaloric effect [41-44] and generally, the metamagnetic transition is responsible of these anomalies. Below T_c , the inverse MCE arises from AFM superexchange interaction between Mn and Nd.

4. Conclusion

In conclusion, we have studied the structural, magnetic and magnetocaloric properties and phase stability in polycrystalline $\text{Nd}_{0.5}\text{Ca}_{0.4}\text{M}_{0.1}\text{MnO}_3$ (with $M=\text{Na, K}$) manganites. Rietveld refinement indicates that all samples are single phase and crystallize in the orthorhombic structure with $Pnma$ space group. As shown in the SEM photographs, a good crystallinity has been observed for both samples even when they were sintered at 1000 °C, which is about 300 °C lower than the normal sintering temperature of an undoped sample. With the increase of the average cationic radius $\langle r_A \rangle$ in the A site, the CO phase gradually melts (NCKMO case) and the long-ranged CO/AFM phase transforms into a short-ranged CO/AFM phase which is metastable. As well, FC and ZFC magnetization curves reflect the existence of competing FM and AFM interactions resulting in the formation of a frustrated spin-glass-like at low temperature. The applied field dependence of magnetization and the temperature dependence of magnetic entropy change confirm the phase-separated nature and the metamagnetic transition of our both samples.

References

- [1] R. von Helmolt, J. Wecker, B. Holzapfel, L. Schultz, K. Samwer, Phys. Rev. Lett. 71 (1993) 2331.
- [2] S. Jin, T. H. Tiefel, M. McCormack, R. A. Fastnacht, R. Ramesh, L. H. Chen, Science. 264 (1994) 413.
- [3] J. Z. Sun, W. J. Gallagher, P. R. Duncombe, L. Krusin-Elbaum, R. A. Altman, A. Gupata, Y. Lu, G. Q. Gong, G. Xiao, Appl. Phys. Lett. 69 (1996) 3266.
- [4] S. Mori, C. H. Chen, S. -W. Cheong, Nature (London). 392 (1998) 437.

- [5] N. R. Rao, A. K. Cheetham, *Science*. 276 (1999) 911.
- [6] Y. Tokura, N. Nagoza, *Science*. 288 (2000) 462.
- [7] P. Schiffer, A. P. Ramirez, W. Bao, S. W. Cheong, *Phys. Rev. Lett.* 75 (1998) 3336.
- [8] Y. Tomioka, A. Asamitsu, Y. Moritomo, H. Kuwahara, Y. Tokura, *Phys. Rev. Lett.* 74 (1995) 5108.
- [9] H. Kuwahara, Y. Tomioka, A. Asamitsu, Y. Moritomo, Y. Tokura, *Science*. 270 (1995) 173.
- [10] T. Vogt, A.K. Cheetham, R. Mahendiran, A.K. Raychaudhuri, R. Mahesh, C.N.R. Rao, *Phys. Rev. B*. 54 (1996) 15303.
- [11] F. Millange, S. De Brion, G. Chouteau, *Phys. Rev. B*. 62 (2000) 5619.
- [12] F. Dupont, F. Millange, S. De Brion, A. Janossy, G. Chouteau, *Phys. Rev. B*. 64 (2001) 220403.
- [13] Run-Wei. Li, Ji-Rong. Sun, Qing-An. Li, Shai-Ying. Zhang, Bao-Gen. Shen, *J. Magn. Magn. Mater.* 265 (2003) 248.
- [14] J.E. Gordon, R.A. Fisher, Y.X. Jia, N.E. Phillips, S. F. Reklis, D.A. Wright, A. Zettl, *Phys. Rev. B*. 59 (1999) 127.
- [15] G. Ayan, G. Arindam, A.K. Raychaudhuri, S. Parashar, A.R. Raju, C.N.R. Rao, *Appl. Phys. Lett.* 75 (1999) 21.
- [16] R. Mahesh, R. Mahendiran, A.K. Raychaudhuri, C.N.R. Rao, *J. Solid State Chem.* 114 (1995) 297.
- [17] H.Y. Hwang, S.W. Cheong, P.G. Radaelli, M. Marezio, B. Batlogg, *Phys. Rev. Lett.* 75 (1995) 914.
- [18] A. Maignan, Ch. Simon, V. Caignaret, B. Raveau, *Solid State Commun.* 96 (1995) 632.
- [19] L.M. Rodrigez-Martinez, J.P. Attfield, *Phys. Rev. B*. 54 (1996) 15622.
- [20] F. Damay, C. Martin, A. Maignan, B. Raveau, *J. Appl. Phys.* 82 (1997) 6181.
- [21] H. Trabelsi, M. Bejar, E. Dhahri, M.P.F. Graça, M.A. Valente, M.J. Soares, N.A. Sobolev, *Appl. Surf. Sci.* 426 (2017) 386.
- [22] H.M. Rietveld, *J. App. Cryst.* 2 65 (1969).
- [23] T. Roisnel, J. Rodriguez-Carvajal, Computer program FULLPROF, LLB-LCSIM, 2003.
- [24] H. Trabelsi, M. Bejar, E. Dhahri, M. Sajieddine, K. Khirouni, P.R. Prezas, B.M.G. Melo, M.A. Valente, M.P.F. Graça, *J Alloys Compd.* 723 (2017) 894.
- [25] S. Chamekh, A. Bouabellou, Y. Elerman, M. Kaya, I. Dincer, *J. New Technol. Mater.* 07, N°02 (2017) 22.
- [26] V.M. Goldschmidt, *Naturwissenschaften.* 14 (1926) 477.
- [27] H. Trabelsi, M. Bejar, E. Dhahri, M. Sajieddine, M.A. Valente, A. Zaoui, *J. Alloys Compd.* 680 (2016) 560.
- [28] H. Trabelsi, M. Bejar, E. Dhahri, M.P.F. Graça, M.A. Valente, K. Khirouni, *Physica E Low Dimens Syst Nanostruct.* 99 (2018) 75.
- [29] M.R. Lees, J. Beratt, G. Balakrishnan, D.MC.K. Paul, M. Yethiraj, *Phys. Rev. B.* 52 14303 (1995).
- [30] A.P. Ramirez, P. chiffer, S-W. Cheong, W. Bao, T.T.M. Palstra, P.L. Gammel, D.J. Bishop, B. Zegarski. *Phys. Rev. Lett. B.* 76 (1996) 3188.
- [31] F. S. Shokr, M. Hussein, E. Dhahri, *J. New Technol. Mater.* 06, N°02 (2016) 24.
- [32] A. Biswas, I. Das, C. Majumdar, *J. Appl. Phys.* 98 (2005) 124310.
- [33] Y. Tokura, Y. Tomioka. *J. Magn. Magn. Mater.* 200 (1999) 1.
- [34] L.M. Rodriguez-Martinez, J.P. Attfield, *Phys. Rev. B.* 54 (1996) 15622.
- [35] F. Damay, C. Martin, A. Maignan, B. Raveau, *J. Appl. Phys.* 82 (1997) 6181.
- [36] I.O. Troyanchuk, V.A. Khomchenko, H. Szymczak, M. Baran, *JETP.* 97 (2003) 1231.
- [37] S. Zouari, E. K. Hlil, M. L.kahn, M. Ellouze, F. Elhalouani, *J. New Technol. Mater.* 06, N°02 (2016) 19.
- [38] M. Aparnadevi, R. Mahendiran, *J. Appl. Phys.* 113 (2013) 013911.
- [39] V.B. Naik, R. Mahendiran, *J. Appl. Phys.* 110 (2011) 053915.
- [40] S.K. Banerjee, *Phys. Lett. A.* 12 (1964) 16.
- [41] V.S. Kolat, T. Izgi, A.O. Kaya, N. Bayri, H. Gencer, S. Atalay, *J. Magn. Magn. Mater.* 322 (2010) 427.
- [42] D.S. Rana, D.G. Kuberkar, M. Tonouchi, S.K. Malik, *J. Magn. Magn. Mater.* 310 (2007) 184.
- [43] A. Biswas, T. Samanta, S. Banerjee, I. Das, *J. Appl. Phys.* 103 (2008) 013912.
- [44] A. Biswas, T. Samanta, S. Banerjee, I. Das, *Appl. Phys. Lett.* 92 (2008) 212502.